07,19

Pressure-Dependent Elastic, Mechanical, and Ultrasonic Analysis of CaAuBi Compound

© A.K. Prajapati, S. Rai, P.K. Yadawa

Department of Physics, Prof. Rajendra Singh (Rajju Bhaiya) Institute of Physical Sciences for Study and Research,
V.B.S. Purvanchal University,
Jaunpur, 222003 India

E-mail: aadeshbhu83@gmail.com

Received: April 12, 2022
Revised: June 13, 2022
Accepted: June 14, 2022

The Lennard–Jones potential model is used to investigate the effects of pressure on the elastic and ultrasonic properties of CaAuBi half-Heusler compound. Potential model technique approaches is used to evaluate second- and third-order elastic constants of CaAuBi compound at various pressures (0–15 GPa). The pressure dependence of elastic constants is studied and it has been observed that the elastic constants of the half-Heusler CaAuBi compound increase monotonically as pressure is increased. The hexagonal half-Heusler CaAuBi compound is mechanically stable at different pressures according to Born's elastic stability criteria. The Voigt–Reuss–Hill method was used to compute elastic parameters such as Young's modulus Y, shear modulus G, bulk modulus B, and Poisson's ratio ν under various pressures. For the provided pressure range, the second-order elastic constants were also utilized to determine ultrasonic velocities along with z-axis at various angles. The half-Heusler CaAuBi compound's hardness, ultrasonic attenuation, melting temperature, and anisotropy are also determined. The computation have been also satisfactory in estimating the thermal conductivity $k_{(\min)}$ and Debye average velocity under varied pressure.

Keywords: elastic properties, thermal conductivity, ultrasonic properties, thermo-physical properties.

DOI: 10.21883/PSS.2022.10.54242.014

1. Introduction

The XYZ formula is used to describe the half-Heusler structural family of ternary compounds (space group F43m, prototype MgAgAs), in which X is typically a rare-earth or transition metal, Y is a transition metal, while Z is a main-group element. X atoms are crammed into YZ zinc blende lattice structure in this cubic structural type [1,2]. Many of the compounds have been studied for thermo-electric & spintronic technologies and superconductivity has been reported for some of them [3–5]. The structural type of essentially all half-Heusler compounds has 18 total valence electrons, and this parameter encompasses a wide range of constituent materials [1]. More specifically, experimentally observed phase transitions in various ternary systems have proven structural proximities between the half-Heusler type of structure and thus the LiGaGe and ZrBeSi structure types. Under high-pressure circumstances, the compounds VCoSb and VFeS that crystallise in the half-Heusler type of structure under standard pressure have been stabilised in a ZrBeSi-type structure [6]. High-temperature and low-temperature phases of the combination YbAuBi have been seen in LiGaGe and half-Heusler structures, respectively [7]. These findings show that infusing energy through half-Heusler systems can reveal incipient structural instabilities. Half-Heusler compounds are structurally proximal to numerous other structure types, according to trends in crystal structures among many groups of related compounds. The compounds with smaller rare-earth elements crystallise in the half-Heusler structure type, while those with bigger rare-earth elements crystallise in the LiGaGe structure type, e.g., inside this REAuSn family (where RE is a rare-earth metal). LiGaGe is a hexagonal variation of the half-Heusler structural type, with X atoms packed into a hexagonal YZ wurtzite sub-lattice instead of a cubic YZ zinc blende sub-lattice [2]. A similar trend is seen in the REAuPb family, but the compounds containing the bigger RE elements crystallise in the ZrBeSi structure type instead of the LiGaGe structure type. The ZrBeSi structural type can be viewed of as a LiGaGe variation with rectangular honeycomb-like YZ layers rather than a puckered YZ sub-lattice [6]. The hexagonal ZrNiAl and orthorhombic TiNiSi structural types impose additional distortions on the YZ sub-lattice, according to studies of other ternary 18 electron systems. These patterns suggest that even little relative size as well as chemistry of the individual elements can cause structural alterations in these systems. SrAuBi and BaAuBi, CaAuBi's chemical analogues, both crystallise in the ZrBeSi type of structure. EuAuBi possesses the LiGaGe structural type among divalent REAuBi compounds, while YbAuBi has temperature-dependent half-Heusler and LiGaGe-type phases. CaAuBi has previously been investigated for high/low-temperature phases, and only the single half-Heusler phase had been discovered [7]. Nonetheless, the wide range of structure types identified in chemically related compounds to CaAuBi motivates more research into structural transitions inside the CaAuBi system. Powder synchrotron diffraction patterns taken at pressures up to 15 GPa reveal a structural transition in CaAuBi from a previously unreported phase in the cubic half-Heusler type

of structure to a previously unknown phase in the hexagonal LiGaGe structure type. For the cubic and hexagonal forms of CaAuBi with pressure, we offer comprehensive structural solutions and total energy estimates [8,9].

In this study, we only focused on the pressure-dependent mechanical, elastic, and thermo-physical properties of CaAuBi compound. Half-Heusler compound CaAuBi will contribute in the study of CaAuBi compound mechanical behavior, as well as serve a significant role in the creation of production apparatus with effective physical properties under reasonable working conditions. We evaluated pressure-dependent ultrasonic velocity, acoustic coupling constants, ultrasonic attenuation (UA) coefficient, and elastic stiffness constant and thermal relaxation time for CaAuBi compound in the present research work. Poisson's ratio ν, Young's modulus Y, bulk modulus B, shear modulus G, and Pugh's ratio B/G were also calculated and analyzed for this CaAuBi compound.

2. Theory

There exist several approaches to analyses high-order elastic factors of hexagonal materials. According to present our effort, the Lennard-Jones interaction potential approaches was using for the evaluation for six second- and ten third-order elastic constants (SOECs and TOECs).

Higher-order elastic constants of hexagonal structured materials are a function of lattice parameters, according to the potential model approach to evaluation. The following formulas can be used to calculate the SOECs [10,11]:

$$C_{IJ} = \frac{\partial^2 U}{\partial e_I \partial e_J}, \quad I, J = 1, \ldots, 6, \tag{1}$$

$$C_{IJK} = \frac{\partial^3 U}{\partial e_I \partial e_J \partial e_K}, \quad I, J, K = 1, \ldots, 6, \tag{2}$$

where $e_I = e_{ij}$ $(i, j = x, y, z, I = 1, \ldots, 6)$ is a component of the strain tensor, and U represents elastic energy density. For hexagonal closely packed structural materials, Eqs (1) and (2) lead to SOEC and TOEC [11,12].

$$\left.\begin{array}{ll} C_{11} = 24.1p^4C' & C_{12} = 5.918p^4C' \\ C_{13} = 1.925p^6C' & C_{33} = 3.464p^8C' \\ C_{44} = 2.309p^4C' & C_{66} = 9.851p^4C' \end{array}\right\}, \tag{3a}$$

$$\left.\begin{array}{l} C_{111} = 126.9p^2B + 8.853p^4C' \\ C_{112} = 19.168p^2B - 1.61p^4C' \\ C_{113} = 1.924p^4B + 1.155p^6C' \\ C_{123} = 1.617p^4B - 1.155p^6C' \\ C_{133} = 3.695p^6B \quad C_{155} = 1.539p^4B \\ C_{144} = 2.309p^4B \quad C_{344} = 3.464p^6B \\ C_{222} = 101.039p^2B + 9.007p^4C' \quad C_{333} = 5.196p^8B \end{array}\right\}. \tag{3b}$$

Here, $p = c/a$ is axial ratio;

$$C' = \chi \cdot a/p^5; \quad B = \psi a^3/p^3;$$

$$\chi = (1/8)[\{nb_0(n-m)\}/\{a^{n+4}\}],$$

$$\psi = -\chi/\{6a^2(m+n+6)\},$$

m and n are integer quantities chosen below; b_0 is the Lennard–Jones parameter. The pressure affects the lattice properties of CaAuBi compound.

In a hexagonal structured crystal, the ultrasonic longitudinal and shear wave velocities (V_L and V_S) for wave propagation along a z-axis are given by the equations [12]:

$$V_L = \sqrt{\frac{C_{33}}{\rho}}, \tag{4}$$

$$V_S = \sqrt{\frac{C_{44}}{\rho}}. \tag{5}$$

The density of hexagonally structured material d can be calculated using the formula below [13]:

$$d = 2Mn/3\sqrt{3}a^2cN_A, \tag{6}$$

where n, M, and N_A represent atoms per unit cell, molecular weight of the compound, and Avogadro number, respectively.

Because ultrasonic velocities are related to elastic constants, Debye average velocity V_D is an important measure in low temperature physics, defined as [12]:

$$V_D = \left[\frac{1}{3}\left(\frac{1}{V_L^3} + \frac{1}{V_{S_1}^3} + \frac{1}{V_{S_2}^3}\right)\right]^{-1/3}. \tag{7}$$

Through Debye average velocity, elastic constants are related to Debye temperature T_D in an indirect way [14]:

$$T_D = \hbar V_D (6\pi^2 n_a)^{\frac{1}{3}}/k_B, \tag{8}$$

where k_B and n_a are the Boltzmann constant and atomic concentration constant, respectively. The energy distribution of thermal phonons is disrupted by the propagation of ultrasonic waves. Through the relaxing mechanism, it achieves equilibrium. Thermal relaxation time τ is defined as the time it takes for thermal phonons to re-establish themselves after an ultrasonic wave has propagated. It is directly connected to thermal conductivity k, Debye average velocity, and specific heat C_V [11,15]:

$$\tau = \tau_S = \tau_L/2 = \frac{3k}{C_V V_D^2}. \tag{9}$$

The shear modulus and bulk modulus were calculated using the methods of Voigt and Reuss [16,17]. The Voigt and Reuss techniques use unvarying stress and unvarying strain computations, respectively. Furthermore, using Hill's approaches, the average values of both methodologies were

used to compute the resulting values of B and G [18]. Young's modulus and Poisson/s ratio ν are calculated using the bulk and shear modulus values [19,20]. For the evaluation of Y, B, G, and ν the following expressions were considered.

$$\left.\begin{aligned} &M = C_{11} + C_{12} + 2C_{33} - 4C_{13};\\ &C^2 = (C_{11} + C_{12})C_{33} - 4C_{13} + C_{13}^2;\\ &B_R = \frac{C^2}{M}; \quad B_V = \frac{2(C_{11} + C_{12}) + 4C_{13} + C_{33}}{9};\\ &G_V = \frac{M + 12(C_{44} + C_{66})}{30};\\ &G_R = \frac{5C^2 C_{44} C_{66}}{2[3B_V C_{44} C_{66} + C^2(C_{44} + C_{66})]}\\ &Y = \frac{9GB}{G + 3B}; \quad B = \frac{B_V + B_R}{2};\\ &G = \frac{G_V + G_R}{2}; \quad \nu = \frac{3B - 2G}{2(3B + G)} \end{aligned}\right\} \quad (10)$$

The thermal conductivity of a substance can be calculated using the formula below [21]:

$$k = AMT_D^3\delta^3/\gamma^2 T n^{2/3}, \quad (11)$$

where A is a constant, δ^3 is volume per atom, γ is Grüneisen number, and T is temperature. The constant A is determined by the Grüneisen number and is expressed as follows:

$$A = 2.43 \cdot 10^{-8} \Big/ \left(1 - \frac{0.514}{\gamma} + \frac{0.228}{\gamma^2}\right). \quad (12)$$

The elastic constants C_{11} and C_{33} are correlated to the melting temperatures T_m of hexagonal crystals [22]. The melting point T_m is calculated as follows

$$T_m = 354 + 4.5(2C_{11} + C_{33})/3, \quad (13)$$

where C_{11} and C_{33} are in GPa, and T_m is in K.

As a result, there is a high chance of acoustic phonons and free electrons coupling [12]. For longitudinal (V_L) and shear waves (V_S), the mathematical formulation of UA is as follows

$$\alpha_{long} = \frac{2\pi^2 f^2}{\rho V_L^3}\left(\frac{4}{3}\eta_e + \chi\right), \quad (14)$$

$$\alpha_{shear} = \frac{2\pi^2 f^2}{\rho V_S^3}\eta_e, \quad (15)$$

where f is the frequency of the ultrasonic wave, ρ is the density of hexagonal compound, η_e is the electron viscosity, and χ is the compression viscosity. At higher pressure, both thermoelastic loss and Akhieser's loss are significant for ultrasonic wave attenuation. The equation given below describes the attenuation caused by Akhieser's loss calculated by Yadav *et al.* [12].

$$(\alpha/f^2)_{Akh} = 4\pi \cdot 2\tau E_0(D/3)/2\rho V^3. \quad (16)$$

The ultrasonic wave frequency is represented by f, and the thermal energy density is represented by E_0.

The following equation considers the thermoelastic loss $(\alpha/f^2)_{Th}$:

$$(\alpha/f^2)_{Th} = 4\pi^2\langle\gamma_i^j\rangle^2\frac{kT}{2\rho V_L^5}. \quad (17)$$

The total UA is specified by the subsequent equation as

$$(\alpha/f^2)_{Total} = (\alpha/f^2)_{Th} + (\alpha/f^2)_L + (\alpha/f^2)_S, \quad (18)$$

where $(\alpha/f^2)_{Th}$ is the thermoelastic loss, $(\alpha/f^2)_L$ and $(\alpha/f^2)_S$ are the UA coefficients for the longitudinal wave and shear wave, correspondingly.

3. Results and Discussion

3.1. Higher-order elastic constants

We have evaluated the six SOECs and ten TOECs using interaction potential method in this investigation. Based on synchrotron X-ray diffraction patterns taken under pressures up to 18 GPa, we report a structural phase change of the ternary compound CaAuBi from the known cubic half-Heusler phase to a hexagonal LiGaGe type phase. The hexagonal form of the half-Heusler structural type is LiGaGe. In this study, we only focused on hexagonal phase of CaAuBi compound under the pressure range (0 to 15 GPa). For the CaAuBi compound, the lattice parameters a (basal plane parameter), p (axial ratio), and density ρ are 4.80 to 4.66 Å, 1.65 to 1.48, 9.40 to 11.61 10^3 kg m^{-3} under the pressure range 0−15 GPa. Evaluated value of thermal conductivity ($k_{(min)}$ Erg/cm · s · K) under the same pressure range is shown in Fig. 1 [23]. For CaAuBi compound, the recommended values of m and n are 6 and 7. For the CaAuBi compound, the value of b_0 is taken as $3 \cdot 10^{-63}$ erg cm^7.

The highest elastic constant values were found in the CaAuBi compound, which are crucial for the material because they are linked to the stiffness parameter. In Fig. 2, we can see that SOECs are increasing with pressure. In Fig. 3, we can see that the values of TOECs are negative and negative value of TOECs is increasing with pressure. The UA and related properties are determined using SOECs. The compound CaAuBi has the highest elastic constant values, indicating that it has higher mechanical properties than other compound.

Consequently, they would satisfy the well-known Born−Huang stability rules [24,25], given by Eq. (19), for the hexagonal compound to be stable (Fig. 4).

$$\begin{aligned} &\acute{C}_{44} > 0, \quad \acute{C}_{11} - |\acute{C}_{12}| > 0,\\ &(\acute{C}_{11} + \acute{C}_{12})\acute{C}_{33} - 2\acute{C}_{13}^2 > 0, \end{aligned} \quad (19)$$

where $\acute{C}_{jj} = \acute{C}_{jj} - P$ $(P = 1, 3, 5)$. $\acute{C}_{12} = C_{12} + P$, $\acute{C}_{13} = = C_{13} + P$.

Because the above elastic constant values are positive, this CaAuBi compound meets Born−Huang's mechanical

stability requirements, suggesting that its mechanical stability increases within the given pressure range. Fig. 2 shows how to determine the bulk modulus of compound CaAuBi. The evaluated value of bulk modulus of CaAuBi compound is 28.32 GPa at zero pressure, which is almost the same as

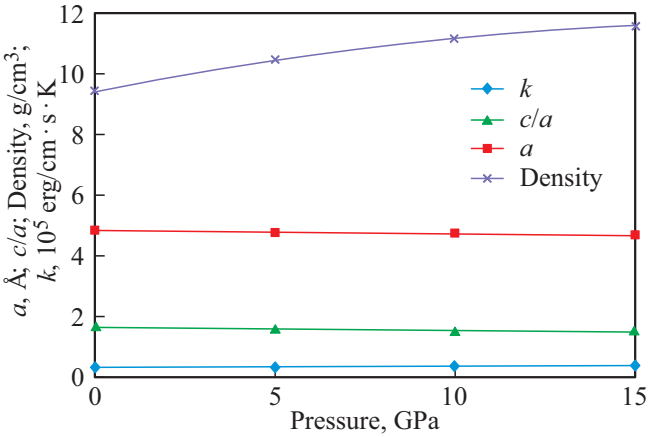

Figure 1. a, c/a, density, and thermal conductivity k *vs* pressure of CaAuBi compound.

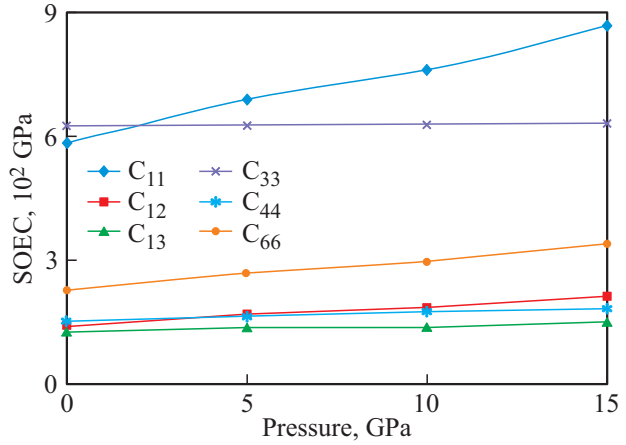

Figure 2. SOECs *vs* pressure of CaAuBi compound.

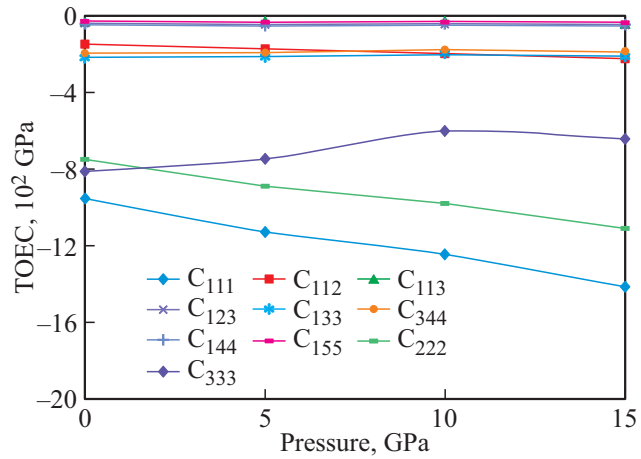

Figure 3. TOECs *vs* pressure of CaAuBi compound.

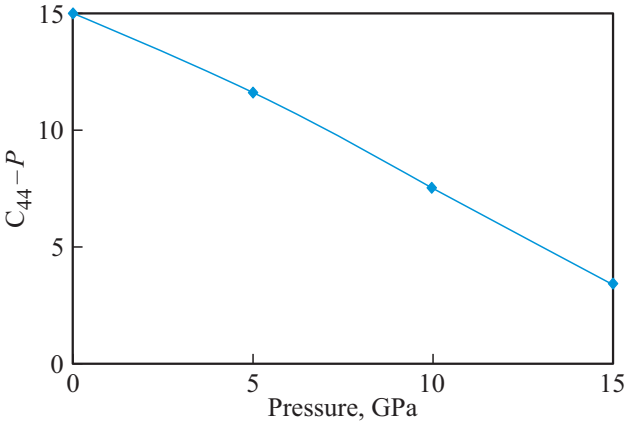

Figure 4. C_{44} — P *vs* pressure of CaAuBi compound.

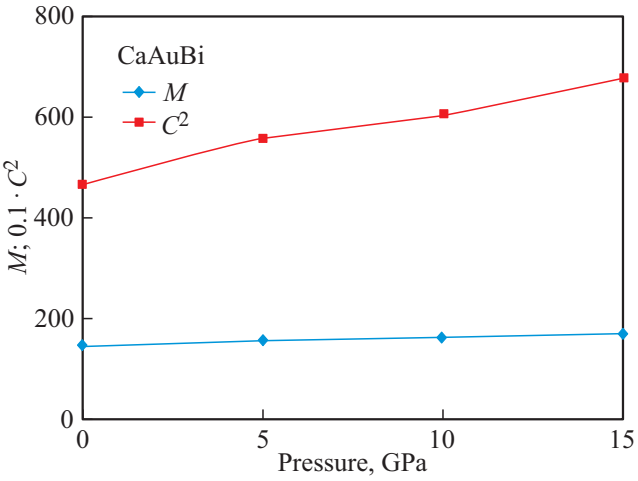

Figure 5. M and C^2 *vs* pressure of CaAuBi compound.

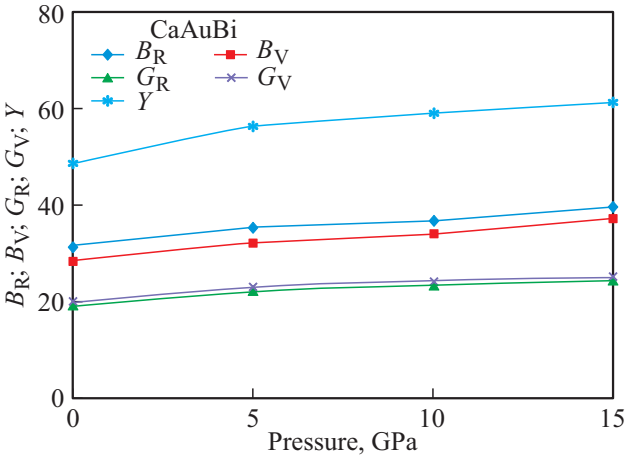

Figure 6. B_R, B_V, G_V, G_R, and Y *vs* pressure of CaAuBi compound.

28.5 GPa calculated by Lilia S. Xie *et al.* [23]. Our approach achieves comparable values of the elastic constants C_{11}, C_{33}, and C_{66}. As a result, there is a fair amount of agreement between the reported and informed values, which is related

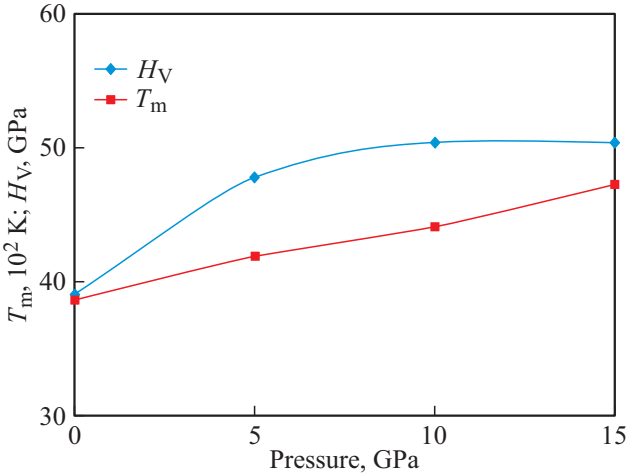

Figure 7. Hardness H_V and melting temperature T_m *vs* pressure of CaAuBi compound.

to elastic constants. As a result, our theoretical methodology for evaluating SOECs of hexagonally structured molecules is well justified. In Fig. 3, we show the calculated TOEC values. TOECs with negative values indicate that the solid is under strain.

The values of Voigt–Reuss' constants (M and C^2), B_R (in $10^{10}\,Nm^{-2}$), B_V (in $10^{10}\,Nm^{-2}$), G_R (in $10^{10}\,Nm^{-2}$), G_V (in $10^{10}\,Nm^{-2}$), Y (in $10^{10}\,Nm^{-2}$) of CaAuBi at different pressures (0 to 15 GPa) are calculated using Eq. (10) and shown in Figs 5 and 6.

All mechanical properties like hardness, brittleness, compressibility, toughness, ductility, and bonding nature are evaluated with the SOECs. The melting temperature was used as a factor for developing improved materials. It is considered as a significant basis for evaluating alloy materials. The analysis of melting temperature has attracted the interest of materials researchers in order to improve the heat resistance of magnesium alloy. In this study, the melting temperature T_m of CaAuBi is investigated. Fig. 7 shows the estimated melting temperature and hardness as a function of pressure. It can be seen that when pressure is increased, the melting temperature increases as well. The unified anisotropic index (A^U), percent anisotropy (A_B and A_G), and shear anisotropic factors (A_1, A_2, and A_3) can always be used to describe anisotropy in elasticity, as shown in the equations below in the table below [26,27].

The table shows that under different pressures of CaAuBi, percent anisotropy A_B is greater than A_G. This indicates

Pressure-dependent anisotropy constants and Poisson's ratio ν of CaAuBi compound

Pressure, GPa	A^U	A_B	A_G	A_1	A_2	A_3	ν
0	0.16	0.05	0.02	0.66	0.66	2.07	0.22
5	0.14	0.04	0.02	0.63	0.63	2.08	0.22
10	0.16	0.02	0.02	0.62	0.62	2.07	0.22
15	0.15	0.02	0.02	0.61	0.61	2.07	0.23

that the shear modulus is more oriented than the bulk modulus. Table also shows the results of A_1, A_2, and A_3 under different pressures. The material is an isotropic crystal if $A_1 = A_2 = A_3 = 1$. It's an anisotropic crystal otherwise, according to the conclusions. The highly single crystal anisotropy is defined as the departures of the universal anisotropic index A^U from zero at different pressures [28,29].

3.2. Ultrasonic velocity and allied parameters

In this study, the isotropic and mechanical properties of the hexagonally structured material are linked to ultrasonic velocity. For the compound CaAuBi, we estimated V_L, V_S, V_D, and τ. The pressure-dependent C_V values and the thermal energy density E_0 were determined using the physical constant tables and Debye temperatures, as shown in Fig. 9. It shows the values of the temperature-dependent acoustic coupling constants (D_L and D_S).

Fig. 8 shows that the values of D_L are greater even than D_S for compound CaAuBi at all pressures. It means that the conversion of ultrasonic energy into thermal energy is lower

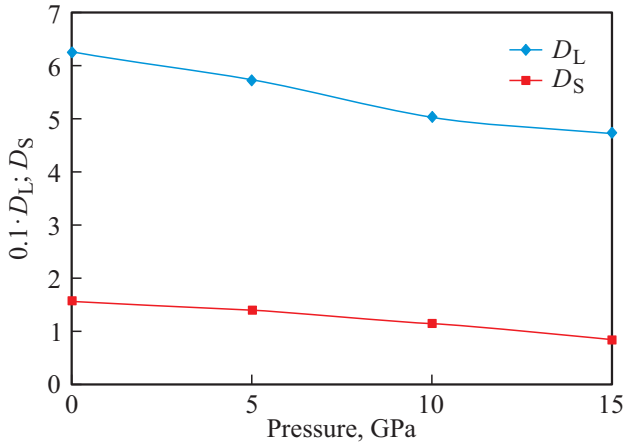

Figure 8. D_L and D_S *vs* pressure of CaAuBi compound.

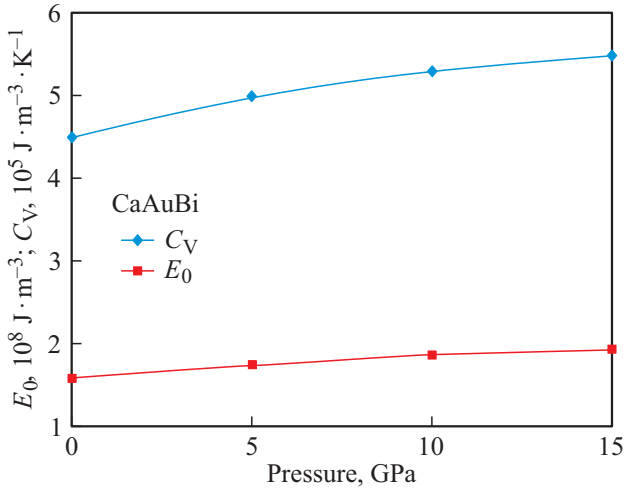

Figure 9. E_0 and C_V *vs* pressure of CaAuBi compound.

for shear ultrasonic waves than for longitudinal ultrasonic waves.

The dependencies of ultrasonic velocities on pressure are shown in Figs 10–13. The velocity V_L of the compound CaAuBi has minima at 0° in Fig. 10, and the velocity V_{S1} has a maximum at angle 45° in Fig. 11. Fig. 12 shows that V_{S2} increases as the z-axis is rotated. The occurrence of SOECs and density causes the irregular behavior of orientation-dependent velocity. The alignment-dependent velocity curves in this study are similar to the orientation-dependent velocity curves seen in other hexagonal materials [28,29]. In the compound CaAuBi, the angle dependency of the velocities is thus justified.

Fig. 13 illustrates the difference in Debye average velocity V_D as a function of the angle made with the crystal's z-axis. For the compound CaAuBi, V_D increases with angle and reaches a maximum at $\theta = 55°$. Because the

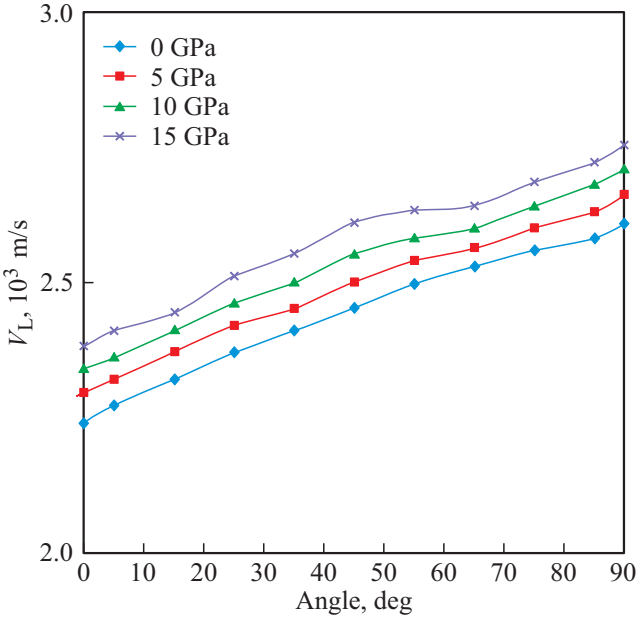

Figure 10. V_L *vs* the angle from z-axis of crystal.

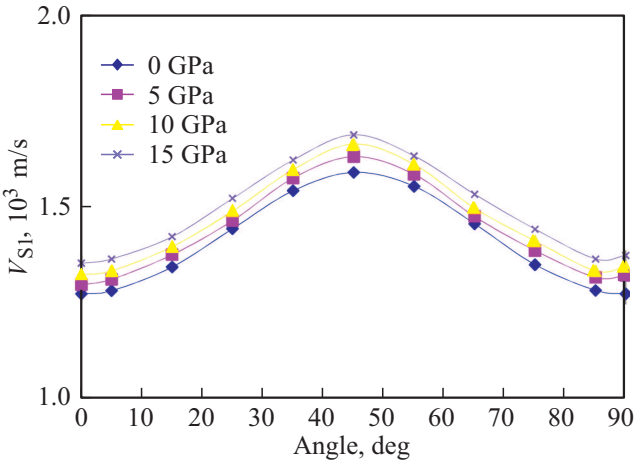

Figure 11. V_{S1} *vs* the angle from z-axis of crystal.

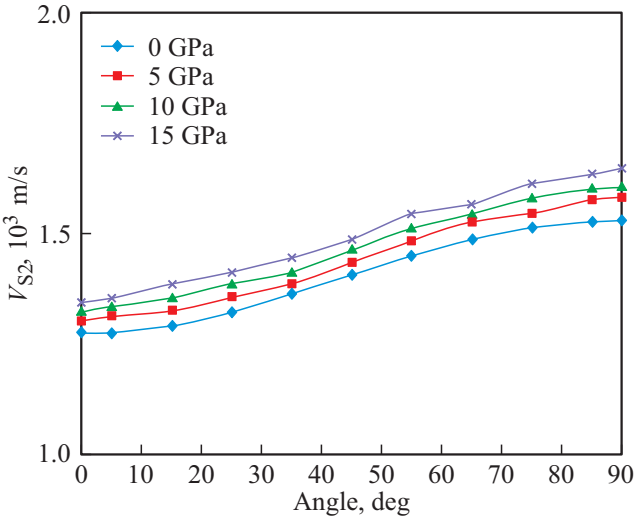

Figure 12. V_{S2} *vs* the angle from z-axis of crystal.

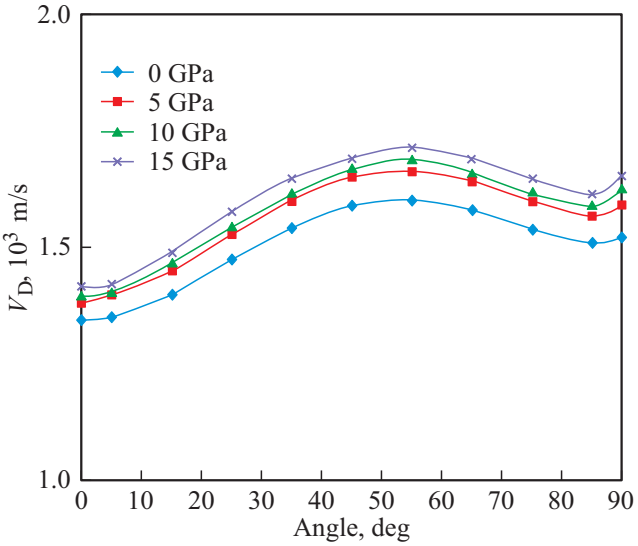

Figure 13. V_{S2} *vs* the angle from z-axis of crystal.

velocities V_L, V_{S1}, and V_{S2} are used in the computation of V_D [30,31], it is understandable that the fundamental ultrasonic velocities influence the variation of Debye's average velocity. A considerable increase in both shear and longitudinal wave velocities, as well as a decrease in quasi-shear wave velocities, results in a maximum value of V_D at 55°. The average sound wave velocity demonstrates that the maximum when a sound wave propagates at 55° degrees with the z-axis of this crystal.

Fig. 14 shows a graph of the evaluated thermal relaxation time as a function of orientation. The reciprocal character of V_D as $\tau \propto 3k/C_V V_D^2$ is measured by angle-dependent curves. Thermal relaxation time for the compound CaAuBi is obviously affected by k. The thermal relaxation time of hexagonal structured materials is in the picosecond range [30,31]. The hexagonal structure of the compound CaAuBi is therefore explained by the computed results. The

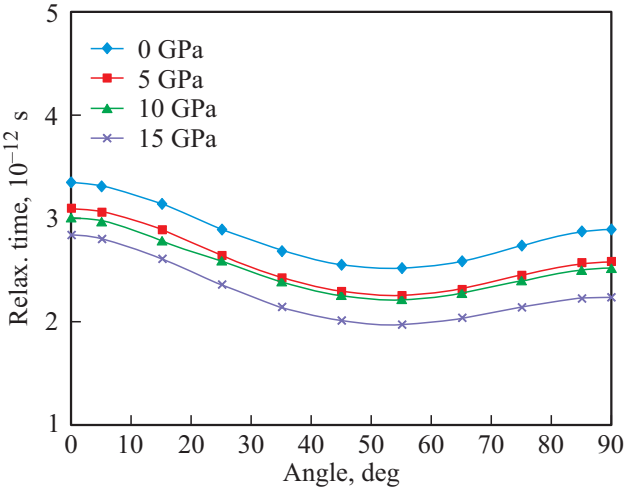

Figure 14. Relaxation time *vs* the angle from *z*-axis of crystal.

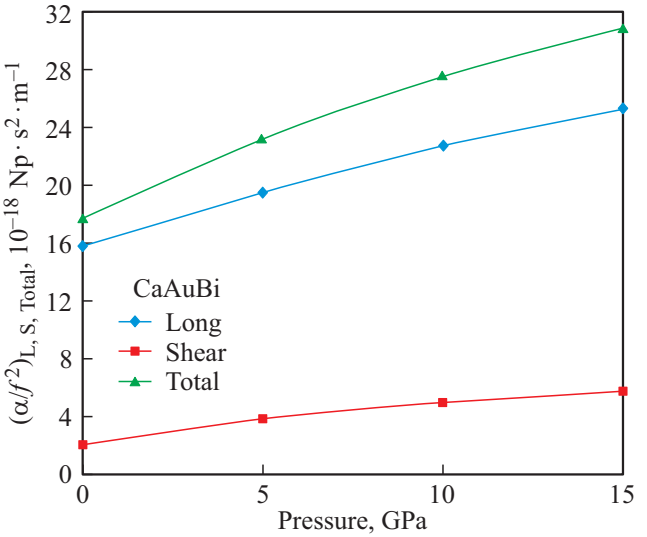

Figure 15. $(\alpha/f^2)_L$, $(\alpha/f^2)_S$, and $(\alpha/f^2)_{Total}$ *vs* the pressure of CaAuBi compound.

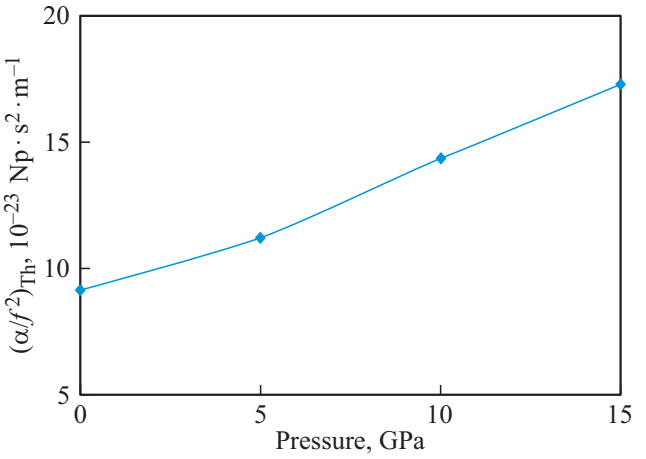

Figure 16. $(\alpha/f^2)_{Th}$. *vs* the pressure of CaAuBi compound.

lowest value of thermal relaxation time for wave propagation along 55° indicates that the re-establishment time for thermal phonon equilibrium distribution will be shortest for wave propagation in this direction due to phonon−phonon (p−p) interaction and thermal relaxation, UA occurs.

3.3. Ultrasonic attenuation due to phonon−phonon interaction and thermal relaxation phenomena

When calculating UA, the wave is assumed to propagate down the *z*-axis of the CaAuBi compound. The attenuation coefficient divided by frequency squared $(\alpha/f^2)_{Akh}$ is calculated for the longitudinal wave $(\alpha/f^2)_L$ and for the shear wave $(\alpha/f^2)_S$ using Eqs (14−16). Figs 15, 16 presented values of the pressure-dependent longitudinal, shear, and total attenuation of the CaAuBi.

The ultrasonic wave is expected to propagate along the crystal's *z*-axis in this study. It is evident that the Akh. Type of energy losses $(\alpha/f^2)_{Akh}$ is proportional to D, E_0, τ, and V^{-3}, see Eq. (16). As a result, E_0 and k have a significant impact on Akhieser losses in CaAuBi.

As a result, the increase in UA is caused by a decrease in thermal conductivity. As a result, it is the p−p interaction that affects UA; due to a lack of theoretical/experimental data of UA, we could not compare.

Eq. (17) shows that the thermoelastic loss for compound CaAuBi is substantially lower than Akhieser loss, as well as the total attenuation using Eq. (18). UA related to p−p interaction for longitudinal wave and shear wave is the major factor. The key factors that influence total attenuation are thermal conductivity and thermal energy density. Thus, at given pressure range, compound CaAuBi behave as their purest form and are further ductile, as evidenced by the minimum attenuation, despite the fact that compound CaAuBi compounds are least ductile. As a result, the compound CaAuBi compound will have the least impurity at ambient temperature. Because the compound CaAuBi has the highest velocities at 15 GPa, $\alpha \propto V^3$ should be maximum at this pressure, and the materials should be the most ductile. At a pressure range of 0 to 15 GPa, the minimum values of UA for the compound CaAuBi defends its hexagonal type structural state, which is quite stable.

4. Conclusion

The pressure-dependent mechanical and thermodynamic characteristics of the CaAuBi are investigated using the simple interaction potential approach at pressures varies from 0 to 15 GPa in this study. The concept of determining higher-order elastic coefficients for hexagonally structured CaAuBi compounds based on a simple interaction potential technique is still applicable at different pressure. Born−Huang stability criteria show that the mechanical stability of CaAuBi is increasing with pressure within the pressure range. The Pugh's ratio indicates that the

hexagonal CaAuBi compound is ductile at both ambient and high pressure, and that the ductility of CaAuBi compound increases as pressure increases. Furthermore, we noticed that CaAuBi compound has a significant anisotropy at 0 GPa, which becomes stronger with increasing pressure. With increased pressure, the Debye temperature increases well as. The calculated melting temperature and hardness of CaAuBi are increasing with pressure. It can be seen that when pressure is increased, the melting temperature increases as well. For CaAuBi, τ is found to be of the order of picoseconds, which defends their hexagonal structure. As τ has smallest value along $\theta = 55°$, at all pressures, the time for re-establishment of symmetry spreading of phonons will be minimum, for the wave propagation in this direction. Over total attenuation, UA caused by p−p interaction mechanism is dominant and is a leading factor of k. At greater pressures, CaAuBi compound behaves as its pure state and is more flexible, as seen by the smallest attenuation.

The research could help with CaAuBi compounds processing and non-destructive characterization. These studies will form a basis for further research into the essential thermo-physical features of various compounds.

Funding

No funding was received to assist with the preparation of this manuscript.

Conflict of Interest

The authors declare that they have no conflicts of interest.

References

[1] T. Graf, C. Felser, S.S.P. Parkin. Prog. Solid State Chem. **39**, *1*, 775 (2011).
[2] F. Casper, R. Seshadri, C. Felser. Physica Status Solidi A **206**, *5*, 1090 (2009).
[3] G. Goll, M. Marz, A. Hamann, T. Tomanic, K. Grube, T. Yoshino, T. Takabatake. Physica B: Phys. Condens. Matter **403**, *5−9*, 1065 (2008).
[4] N.P. Butch, P. Syers, K. Kirshenbaum, A.P. Hope, J. Paglione. Phys. Rev. B **84**, *22*, 220504 (2011).
[5] F.F. Tafti, T. Fujii, A. Juneau-Fecteau, S.R. de Cotret, N. Doiron-Leyraud, A. Asamitsu, L. Taillefer. Phys. Rev. B **87**, *18*, 184504 (2013).
[6] Y. Noda, M. Shimada, M. Koizumi. Inorg. Chem. **18**, *11*, 3244 (1979).
[7] F. Merlo, M. Pani, M.L. Fornasini. J. Less Common Metals **166**, *2*, 319 (1990).
[8] R. Marazza, D. Rossi, R. Ferro. J. Less Common Metals **138**, *2*, 189 (1988).
[9] A. Iandelli. Rev. Chim. Min. **24**, *1*, 28 (1987).
[10] D.K. Pandey, P.K. Yadawa, R.R. Yadav. Mater. Lett. **61**, *30*, 5194 (2007).
[11] P.K. Yadawa. Arabian J. Sci. Eng. **37**, *1*, 255 (2012).
[12] N. Yadav, S.P. Singh, A.K. Maddheshiya, P.K. Yadawa, R.R. Yadav. Phase Transit. **93**, *9*, 883 (2020).
[13] D.K. Pandey, S. Pandey. Ultrasonics: A technique of material characterization. Sciyo Publisher, Sciyo, Croatia (2010). Pp. 397−407.
[14] S.O. Pillai. Solid State Physics: Crystal Physics. New Age International Publisher, USA (2005). Pp. 100−134.
[15] D. Singh, D.K. Pandey, P.K. Yadawa, A.K. Yadav. Cryogenics **49**, *1*, 12 (2009).
[16] P.K. Yadawa. J. Pure. Appl. Ultrasonics **40**, *1*, 16 (2018).
[17] P.K. Yadawa, D. Singh, D.K. Panday, R.R. Yadav. Open Acoustics J. **2**, 61 (2009).
[18] R. Hill. Proc. Phys. Soc. A **65**, *5*, 349 (1952).
[19] N. Turkdal, E. Deligoz, H. Ozisik, H.B. Ozisik. Phase Transit. **90**, *6*, 598 (2017).
[20] P.F. Weck, E. Kim, V. Tikare, J.A. Mitchell. Dalton Trans. **44**, 18769 (2015).
[21] D.T. Morelli, G.A. Slack. High lattice thermal conductivity solids in high thermal conductivity of materials. Springer Publisher, USA (2006). Pp. 37−68.
[22] M.E. Fine, L.D. Brown, H.L. Marcus. Scripta Metallurgica **18**, *9*, 951 (1984).
[23] L.S. Xie, L.M. Schoop, S.A. Medvedev, C. Felser, R.J. Cava. Solid State Sci. **30**, 6 (2014).
[24] N. Yadav, S.P. Singh, A.K. Maddheshiya, P.K. Yadawa, R.R. Yadav. Phase Transit. **93**, *9*, 883 (2020).
[25] C.P. Yadav, D.K. Pandey, D. Singh. Indian J. Phys. **93**, *9*, 1147 (2019).
[26] A.L. Ivanovskii. Int. J. Refract. Met. Hard Mater. **36**, 179 (2013).
[27] A. Guechi, A. Merabet, M. Chegaar, A. Bouhemadou, N. Guechi. J. Alloys Compd. **623**, 219 (2015).
[28] S.I. Ranganathan, M. Ostoja-Starzewski. Phys. Rev. Lett. **101**, *5*, 055504 (2008).
[29] K.B. Panda, K.S. Ravi Chandran. Comput. Mater. Sci. **35**, *2*, 134 (2006).
[30] S.P. Singh, G. Singh, A.K. Verma, P.K. Yadawa, R.R. Yadav. Pramana — J. Phys. **93**, 83 (2019).
[31] A.K. Jaiswal, P.K. Yadawa, R.R. Yadav. Ultrasonics **89**, 22 (2018).